# DEVELOPMENT OF AN INNOVATIVE COOLING SYSTEM AT THE COUNTERSHAFT ASSEMBLY STATION

UDC:621.56A59:519.6
Original scientific paper https://doi.org/10.46793/aeletters.2024.9.4.2

**L.E. Espino-De la Rosa[1], H. Arcos-Gutiérrez[2], J.E. García Herrera[2], I.E. Garduño[2], J.A. Betancourt-Cantera[*3]**

[1]Posgrado CIATEQ A.C., Eje 126 No. 225, Industrial Park, San Luis Potosi 78395, Mexico
[2]CONAHCYT-CIATEQ A.C, Eje 126 No. 225, Industrial Park, San Luis Potosi 78395, Mexico
[3]CONAHCYT-InnovaBienestar from Mexico, Science and Technology #790, Saltillo 25290, Coah., Mexico

**Abstract:**
In automotive component manufacturing, temperature gradients are typical at workstations, especially in summer, affecting production processes. Interruptions in production lines are unacceptable, as constant flow is crucial to avoid financial losses. This issue is evident at the assembly station for the countershaft of truck transmissions, which can reach 181.7°C after welding. During summer, downtimes increase due to inadequate cooling process, as indicated by 235 minutes of downtime in May, coinciding with rising temperatures and increased demand in September, highlighting the need for an effective cooling system. This research proposes a novel design to homogenize cooling times for the countershaft. The cooling cabin was designed to fit the shaft dimensions, with air inlets strategically positioned based on assembly geometry, focusing on the hottest area. Numerical simulations using the finite element method integrated a turbulence model to analyze airflow at the cabin's inlet and outlet. The goal was to reduce the shaft temperature from 181.7°C to an ambient range of 28°C to 34°C, minimizing cooling time and reducing downtime. Results showed a successful reduction, achieving 26.9°C.

**ARTICLE HISTORY**
Received: 14 August 2024
Revised: 24 October 2024
Accepted: 1 November 2024
Published: 16 December 2024

**KEYWORDS**
Design and Simulation, Ansys Software, Cooling system, Countershaft, CFD simulation

## 1. INTRODUCTION

Scientific and technological advances have fueled remarkable economic and industrial growth over the past three decades [1-3]. This growth has created a critical need for the efficient transportation of materials and manufactured products, whether for production purposes or delivery to end customers. Various modes of transportation, including sea, air, and land, are employed based on distance and mobility requirements. In Mexico, land transport accounts for approximately 64% of exports and 51% of imports, highlighting its significant role [4]. The challenges of transporting consumed and manufactured goods are undeniably important for the country. The land transport sector is thus of vital significance not only in Mexico but also globally.

Consequently, ensuring the optimal performance of trucks is essential to fulfilling this crucial role [5].

This highlights the critical importance of continuous innovation in designing trucks, both now and in the future. One of the essential elements of a truck is its transmission [6], which is necessary for proper load handling and distribution, particularly in challenging field conditions [7]. The transmission comprises several crucial components, such as the auxiliary gears (countershaft) [8] and the main shaft [9]. These components collaborate to distribute the load according to the chosen speeds are comprised of various subassemblies (shafts and gears), and are joined by welding

*CONTACT: J.A. Betancourt-Cantera, e-mail: jbetancourt@innovabienestar.mx

processes. Some models within the company are joined by one or two welding beads using the Gas Metal Arc Welding (GMAW) process [10,11]. This process is carried out within a welding station using a robot. During this operation, the piece leaves at an average temperature of 181.3°C to continue its journey within the assembly line, passing to a specific area for forced cooling with fans [12] located approximately 1.5 meters away from the components. However, this cooling method is unsuitable since it does not provide direct airflow to the components but only the recirculation of the same air with the same temperature as the environment, between 28°C and 34°C, depending on the year's season.

This inefficient cooling method cannot be controlled, and due to the climatic conditions (very hot in spring and summer), the downtime for this process to complete can be extended up to 90 minutes before the parts can be safely handled at the next assembly station.

To optimize the process, a cooling system that allows control over the times at this station must be implemented. However, space is limited and implementing a commercial cooling system is complicated.

Therefore, the solution to this problem was to develop a cooling system. According to the literature, design and simulation software use contributes significantly to cost reduction and the development of more efficient products, especially in industries such as automotive and aeronautics [13].

As noted by several authors, numerical simulation is fundamental in developing prototypes across various industry sectors, particularly through Computational Fluid Dynamics (CFD) technology [14-20]. Advancements in computer hardware have facilitated the increased use of CFD in the automotive industry. The application of CFD in this sector is extensive; it is employed at various stages of the manufacturing process, beginning in the car design phase, as described by *Kobayashi and Tsobukura* [21]. Additionally, researchers have utilized CFD in studies related to engine cooling [22,23] and other cooling simulations [24]. For instance, *Hasan et al.* [25] employed CFD to investigate the influence of a novel, efficient air-cooling system design to enhance lithium-ion batteries' performance by lowering operating temperatures under different coolant flow rates. *Gammaidoni et al.* [26] analyzed the cooling system of an electric motor using CFD, while *Kim and No* [27] used a CFD-based design to optimize an air-cooled passive decay heat removal system. *Tan et al.* [28] demonstrated that CFD results are in good agreement with experimental outcomes, reporting a maximum relative error of less than 10% in their evaluation of cooling performance. CFD is a powerful tool that enables both the observation of prototype behavior and the detailed analysis of physical interactions. By focusing on variables of interest, such as temperature, this research utilizes dedicated software like ANSYS-FLUENT, known for its exceptional capabilities in this field, and the finite element method [29].

The main objective of this project is to design and simulate an advanced cooling system for the countershaft assembly. This system aims to reduce cooling time while enabling the operator to control the temperature during subsequent operations.

## 2. MATERIALS AND METHODS

The design and simulation of the cooling system were conducted using the ANSYS FLUENT 2023 R2 teaching version. The computations were performed on a computational node with 24 cores and 128 GB of RAM. A Keysight U5857A thermographic camera was utilized to capture thermographic images.

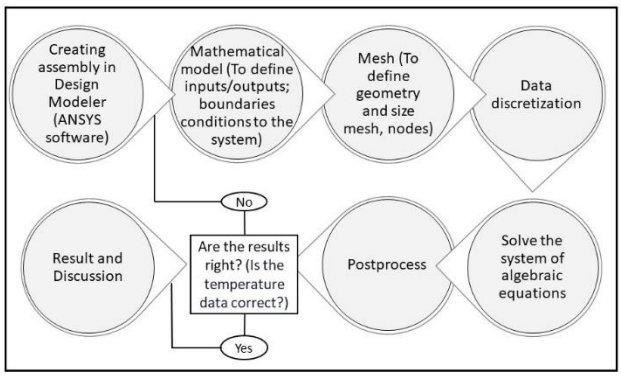


**Fig. 1.** Flow diagram of the experimental development of cooling system [14]

The flow diagram in Fig. 1 presents the methodology for developing the cabin design and conducting the subassembly simulation process. This methodology involved creating a Computing-Aided Design (CAD) design in the design modeler software, serving as the physical model for analyzing the design's physics. Subsequently, a mathematical model, particularly the k-ω SST model, was employed to establish a suitable solution for the analysis, with air inlets at a temperature of 20°C. The complete assembly utilized AISI 4140 steel (42CrMo4 in the EN standard), considering the initial temperature

obtained from the average, 181.7°C for the entire countershaft part. Additionally, aluminium was chosen as the material for the cabin's design.

To validate the data analyzed in this work, Fig. 2 presents a thermographic image of the assembled gear system in the welding station. The figure reveals an output temperature range of 179.5°C to 183.9°C. Multiple measurements were conducted across different parts to establish an average temperature of 181.7°C, thereby minimizing potential measurement errors.

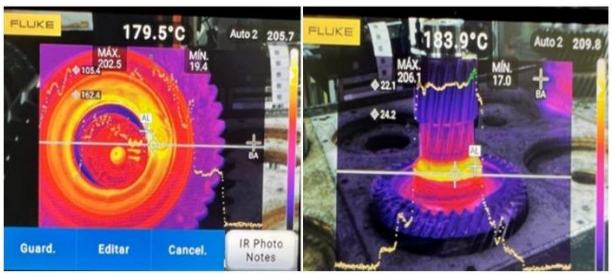


**Fig. 2.** Exit temperature of the shaft and gear welding bead

In addition to the temperature data, a histogram in Fig. 3 illustrates the downtime caused by inadequate cooling processes. Notably, 235 minutes of downtime occurred in May, coinciding with increasing room temperatures. Meanwhile, in September, there was a surge in demand for components. This annual phenomenon highlights that downtime results from the absence of an effective cooling system. Although these specific months suffered the most significant downtime, any disruption in the production line across branches is unacceptable. A seamless production flow is crucial, as options lead to significant economic losses for the company.

| Downtime per month | minutes |
|---|---|
| January | 30 |
| February | 120 |
| March | 25 |
| April | 0 |
| May | 235 |
| June | 95 |
| July | 45 |
| August | 105 |
| September | 450 |
| October | 50 |
| November | 10 |
| December | 65 |
| Total | 1,230 |

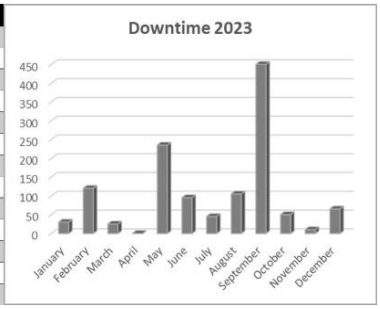


**Fig. 3.** Downtime due to inadequate cooling process

## 2.1 Design of the cabin-Countershaft system

As previously mentioned, and in line with the methodology described in the previous diagram, the design of the confinement cabin is illustrated in Fig. 4, showing the air inlets and outlets. The cabin dimensions are 0.5 x 0.5 x 0.4 meters (length, width, and height), ensuring that the operator can easily insert and handle the assembled component inside the cabin.

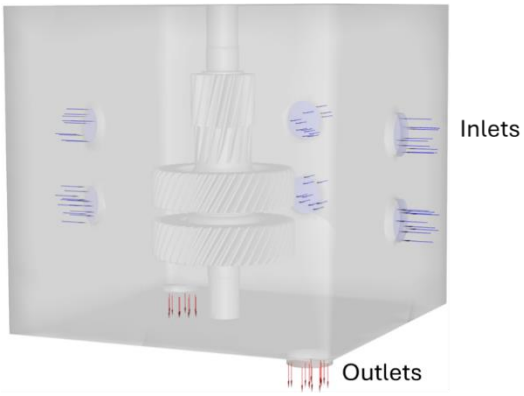


**Fig. 4.** Diagram of airflow inlet and outlet in the cooling cabin

The cabin design features two air vents at the top, four on the side faces, and two additional vents at the bottom and top, positioned centrally on the walls to ensure uniform cooling through the generated turbulent flow. For the cooling system, variables such as the cabin's adiabatic walls and the interaction of the internal air with the system were considered. The air vents were also integrated as an essential part of the system. Thus, the design and simulation of the cooling system were carried out, considering the dimensions of the assembled components. Fig. 5 displays the meshing of the gear-arrow assembly, revealing a complex, unstructured polyhedral mesh geometry. This mesh type was specifically chosen to accommodate the countershaft's intricate features, including triangular, rectangular, and polyhedral shapes. The computational domain was divided into 5,526,980 cells and 598,636 nodes.

## 2.2 Mathematical model

A mathematical model was developed to study the fluidity and heat transfer inside the part and the cabin. A brief description of the different equations and models used is given below.

### *2.2.1 Fundamental Equations*

The fundamental equations that govern this model are the Navier-Stokes equations of continuity and energy for incompressible fluids in Cartesian coordinates and are written as follows:

$$(\nabla \cdot u)=0 \quad (1)$$

$$\rho[\nabla \cdot u]=-\nabla P+\mu_{eff}\nabla^2 u+\rho g \quad (2)$$

$$\frac{\partial}{\partial t}\left(\rho(e+\frac{v^2}{2})\right)+\nabla\cdot\left(\rho v\left(h+\frac{v^2}{2}\right)\right)=$$

$$\nabla\cdot\left(k_{eff}\nabla T-\sum_j h_j\overrightarrow{J_j}+\overline{\overline{\tau_{eff}}}\cdot\vec{v}\right)+S_h \quad (3)$$

where:

$k_{eff}$ is the effective conductivity (K+$k_t$),

$k_t$ is turbulent thermal conductivity,

Y $\overrightarrow{J_j}$ is the diffusion of species flow *j*.

The first terms represent energy transfer by conduction, diffusion, and relative dissipation viscosity. $S_h$ includes the volumetric heat source.

Enthalpy $h$ is defined as an ideal gas as:

$$h=\sum_j Y_j\, h_j \quad (4)$$

and for incomprehensible materials, the contribution for pressure work is included

$$h=\sum_j Y_j\, h_j+\frac{p}{\rho} \quad (5)$$

Model *k-ω* SST standard - this model is defined as follows:

$$\frac{\partial}{\partial t}(\rho k)+\frac{\partial}{\partial x_i}(\rho k u_i)=\frac{\partial}{\partial x_j}\left(\Gamma_k\frac{\partial k}{\partial x_j}\right)+\tilde{G}_k-Y_k+S_k \quad (6)$$

$$\frac{\partial}{\partial t}(\rho\omega)+\frac{\partial}{\partial x_i}(\rho\omega u_i)=\frac{\partial}{\partial x_j}\left(\Gamma_\omega\frac{\partial \omega}{\partial x_j}\right)+G_\omega-Y_\omega+D_\omega+S_\omega \quad (7)$$

In equation 3 $\tilde{G}_k$ represents the generation of turbulent kinetic energy due to gradients in the average velocity, $G_\omega$ represents the generation of $\omega$, $\Gamma_k$, $\Gamma_\omega$ represents the effective diffusivity of *k* and ω, respectively.

$Y_k$ and $Y_\omega$ represents the dissipation of *K* and *ω* due to turbulence, $D_\omega$ represents the term cross-diffusion, $S_k$ and $S_\omega$ are the user-defined source terms.

## 2.3 Considerations of the model

To perform the numerical simulation, the model utilized an air inlet at 18°C as the working fluid, with the countershaft made of AISI 4140 steel. All simulations were conducted in transient, non-isothermal states. Non-slip boundary conditions were applied to all solid walls in the model. The inlet and outlet conditions were set for velocity and pressure, respectively, with a pressure of 1 atm (101,325 Pa) to ensure system equilibrium. The cabin walls were assumed to be adiabatic, while the countershaft temperature was maintained at 181.7°C. Gravity acted only in the specified direction. The physical properties of the fluid, solid, and simulation parameters are provided in Table 1.

**Table 1.** Physical properties of air and AISI 4140 steel

| Phase | Property | Value |
|---|---|---|
| **Air** | Density (kg/m$^3$) | 1.225 |
| | Viscosity [(Kg/(m s)] | 1.79E-05 |
| | Thermal Conductivity[W/(mK)] | 0.0242 |
| | Specific heat (J/ (Kg K) | 1006.43 |
| **Steel** | Density (kg/m3) | 7849.8 |
| | Specific heat (J/ (Kg K) | 435.9 |
| | Thermal expansion coefficient [K$^{-1}$] | 1.17E-05 |
| | Thermal Conductivity [W/(mK)] | 43.33 |

The k-ω SST turbulence model was employed to solve the numerical model over a three-minute simulation period, with the energy equation ensuring a constant temperature within the system. The model equations were discretized using FLUENT computational software, applying the coupled method with an implicit first-order formulation. Additionally, second-order discretization was used for the turbulence model, the Navier-Stokes equations, and the energy equation. The coupling between pressure and velocity was achieved using the SIMPLE method. The convergence criterion was set at 1x10$^{-4}$ or lower. Two case studies were conducted, simulating different scenarios while keeping the width and thickness of the part and the cabin constant throughout the simulations.

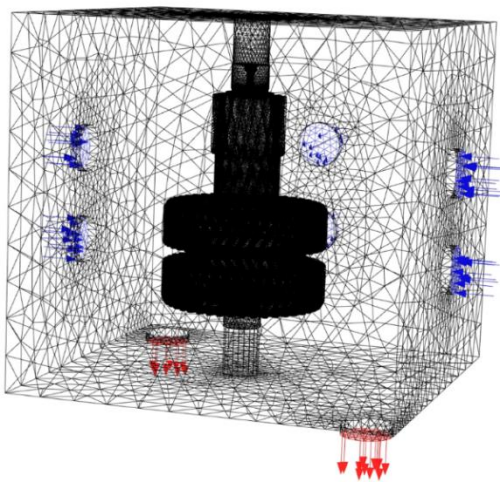

**Fig. 5.** Mesh of the three-dimensional virtual model of the countershaft to scale 1:1

For the assembly, the original serrated geometry shown in Fig. 5 was initially used but later modified to simulate the part as a solid without toothed

diameters. This modification was necessary due to the intricate geometry of the gears, which significantly increased the simulation time. In both case studies, an air velocity of 0.4166 m/s and a temperature of 181.7°C were utilized.

## 3. RESULTS AND DISCUSSION

Figs. 6a, 6b and 6c illustrate the key geometric placements in the cooling cabin design, which ensures efficient airflow by incorporating six air inlets across three sides of the cabin. One side was intentionally left out to allow for door installation, facilitating the insertion and removal of the assembly. The positions of the air inlets and outlets were strategically chosen to align with the placement of the weld seams during assembly. These locations were selected because the hottest part of the component coincides with the weld seams, making effective heat extraction from this area essential.

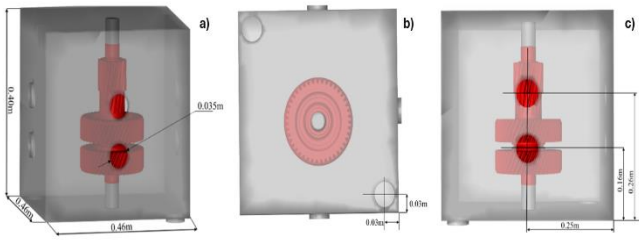


**Fig. 6.** Geometry diagram for a) cabin, b) air inlet on three sides, and c) air outlet top view

Continuing the discussion on the results, Figs. 7a, 7b, and 7c display the temperatures obtained from the simulations. Fig. 7a shows a temperature of 131.3°C, which is significantly lower than the initial temperature of the assembly at the end of the welding station (181.7°C).

This substantial difference of 50.4°C is neither desirable nor optimal. It is important to highlight that the simulation of this design requires a high level of complexity due to the intricate nature of the component, necessitating over 10 million nodes. As a result, even with a moderate mesh size, simulation times were considerably prolonged, leading to unsatisfactory outcomes.

Modifications were made to the assembly design to address this issue by simplifying some detailed features. As mentioned earlier, the arrow and the gears were solid parts. This adjustment enabled two additional simulations, as shown in Figs. 7b and 7c, resulting in 65.1°C and 26.9°C, respectively. Notably, these geometric changes significantly reduced simulation time, allowing us to achieve the desired results from the project's outset.

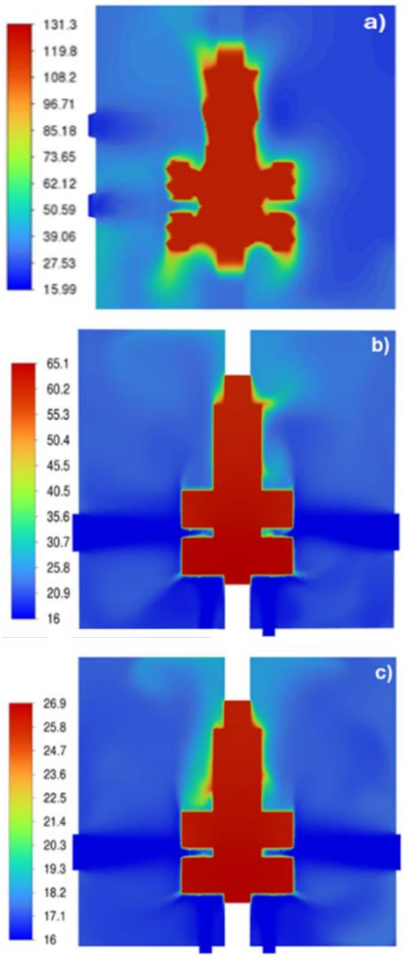


**Fig. 7.** Thermography of the system for a) original geometry, b) modified geometry, and c) modified geometry and reduced simulation time

Fig. 8 shows the vectors resulting from the turbulence of the simulated airflow. These vectors have a similar impact across all three scenarios. However, Fig. 8a reveals an interesting observation: the air inlet gives rise to two significant fluid recirculation zones in the cabin's upper and lower areas. Consequently, a dead zone is formed, characterized by minimal fluid movement. Dead zones are regions within the fluid where interaction with the cabin's surface and the countershaft is minimal or nonexistent, primarily due to little or no fluid movement in these areas. This phenomenon is attributed to the formation of turbulent structures that generate vortices and secondary currents, leading to uneven flow distribution. As a result, low-pressure regions develop in the center of these zones, where the flow is either trapped, circulates slowly, or recirculates, resulting in almost no heat dissipation.

In contrast, at the perimeter of these zones, flow velocities tend to be significantly higher due to the presence of pressure gradients and the effects of centrifugal forces generated by turbulent vortices. This leads to a higher momentum and heat transfer rate to the surrounding walls, creating regions of high heat dissipation. As shown in Fig. 7a, this phenomenon ultimately hinders efficient heat extraction.

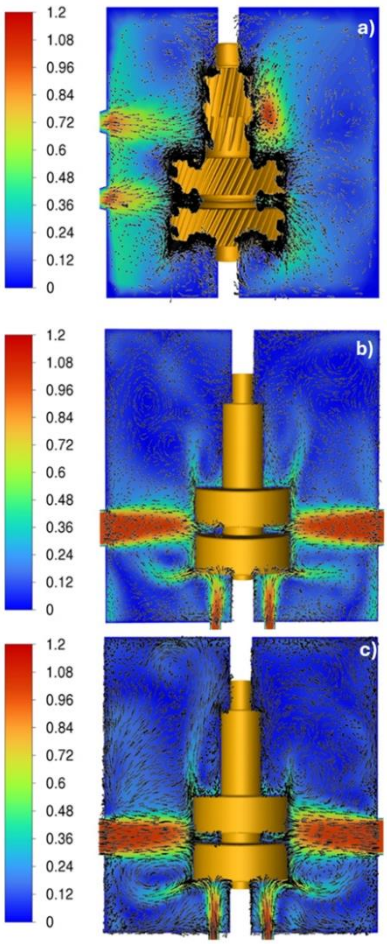


**Fig. 8.** Vectors from airflow for cooling: a) original geometry, b) modified geometry, and c) modified geometry and reduced simulation time.

Figs. 8b and 8c demonstrate that the implemented modifications have effectively created a uniformly turbulent flow within the hottest region identified in the analysis. Additionally, the figures illustrate how this turbulent flow splits into two large recirculation zones in the upper part of the cabin. These zones are crucial in homogenizing the cabin's temperature by transferring motion and heat to cooler regions or air outlets. A high heat, motion, and turbulent kinetic energy exchange between different fluid layers or turbulent structures also characterizes two smaller recirculation zones.

Furthermore, the direct impact of the air jets on the object's thicker sections results in more pronounced temperature gradients, which in turn lead to accelerated heat extraction due to enhanced turbulence and rapid thermal energy exchange between fluid molecules.

## 4. CONCLUSION

This study highlights the methodical analysis of a real problem, in this case, providing a practical solution to the automotive industry through the implementation of the scientific bases for the design, simulation, and optimization of a specific cooling cabin through the study of the physical and fluid properties, as well as the implementation of computational tools such as CFD for analysis. The consideration and study of the temperature-dependent dynamic properties of the fluid in numerical analysis through computational tools such as CFD and its ability to thoroughly examine phenomena with great precision allows for obtaining valuable results from this research, especially in the automotive industry, where saving time in experimentation is vital.

The properties of the fluid significantly influence the results obtained. When adjusted correctly, the k-ε model is especially suitable for simulating heat exchangers, achieving close convergence between numerical and experimental results. Similarly, in designing a cooling cabin, the SST K-ω model has proven to be an indispensable tool for CFD simulation. This formulation combines the strengths of both the k-ε and k-ω models, offering exceptional capability to analyze complex heat transfer phenomena in engineering systems.

The main conclusions from this research are as follows:

1. The innovative cabin design incorporates advanced coupling technology and synchronized welding cycle times, enabling seamless integration with the conveyor system and efficient part production.
2. Experimental data indicate that the new cabin design has significantly improved cooling time, reducing it from one hour and thirty minutes for a batch of 20 pieces to just three minutes per piece.
3. Optimization of the cabin design has significantly reduced part temperatures. By meticulously controlling all parameters and utilizing feedback from previous simulations,

the final simulation achieved a temperature of 26.9°C.

These encouraging results provide the basis for further research involving a more precise and advanced analysis using the Large Eddy Simulation (LES) turbulence model. This model will accurately describe the generation, evolution, and effects of large-scale vortices, turbulent mixing, convective heat transfer, and fluid-structure interactions. These complex phenomena are fundamental for a more concise description of the countershaft cooling process and the temperature distribution in the cabin.

**Acknowledgments**

L.E.E.R. gratefully acknowledges CONAHCyT for the scholarship granted for the postgraduate studies of a master's in advanced manufacturing with industry, Eaton enterprise for the facilities, and CIATEQ A.C. for supporting this project.

H.A.G., J.E.G.H. and I.E.G.O. gratefully acknowledge support from the Investigadores por México – CONAHCYT program through project No. 674. J.A.B.C. gratefully acknowledges support from the Investigadores por México- CONAHCYT program through project No.850.

**CONFLICTS OF INTEREST**

The authors declare no conflict of interest.

**REFERENCES**

[1] M. Pansera, R. Owen, Framing inclusive innovation within the discourse of development: Insights from case studies in India. *Research Policy*, 47(1), 2018: 23–34. https://doi.org/10.1016/j.respol.2017.09.007

[2] A.J. Field, The Most Technologically Progressive Decade of the Century. *American Economic Review*, 93(4), 2003: 1399-1413. https://doi.org/10.1257/000282803769206377

[3] M. Khodaparastan, A.A. Mohamed, W. Brandauer, Recuperation of regenerative braking energy in electric rail transit systems. *IEEE Transactions on Intelligent Transportation Systems*, 20(8), 2019: 2831-2847. https://doi.org/10.1109/TITS.2018.2886809

[4] INEGI, (2021). Conociendo la Industria del Autotransporte de Carga. México: Instituto Nacional de Estadística y Geografía. https://www.inegi.org.mx/contenidos/productos/prod_serv/contenidos/espanol/bvinegi/productos/nueva_estruc/889463903994.pdf (Accessed: 12 August 2024)

[5] C.Z. Asencio Malave, M.Á. Ganchozo López, Costo de Logistica y Rentabilidad en la Empresa de Transporte Tranpsfar S.A, 2022. *Ciencia Latina Revista Científica Multidisciplinar*, 8(1), 2024: 186-204. https://doi.org/10.37811/cl_rcm.v8i1.9410

[6] M. Yolanda, R. Morales, L. Gerardo, S. Vela, Análisis de las características y capacidad de diseño de los vehículos de carga considerando la potencia y torque del motor del vehículo. *SCT*, Publicación técnica No.412, Sanfandila 2014. (In Spanish)

[7] L. Solazzi, D. Bertoli, L. Ghidini, Static and dynamic study of the industrial vehicle transmission adopting composite materials. *Composites Structure*, 316, 2023: 117042. https://doi.org/10.1016/j.compstruct.2023.117042

[8] K.A. Nerstad, W.E. Windish, Countershaft transmission. Patent US 4676116, United States, 1987.

[9] O.C. Duffy, S.A. Heard, G. Wright, Fundamentals of Mobile Heavy Equipment. *Jones & Bartlett Learning*, Burlington, USA, 2019.

[10] M.S. Wêglowski, Y. Huang, Y.M. Zhang, Effect of welding current on metal transfer in GMAW. *Archives of Materials Science and Engineering*, 33(1), 2008: 49-56.

[11] I.A. Ibrahim I. S.A.Mohamat, The Effect of Gas Metal Arc Welding (GMAW) processes on different welding parameters. *Procedia Engineering*, 41, 2012: 1502-1506. https://doi.org/10.1016/j.proeng.2012.07.342

[12] M.J. Cabascango Álvarez, Modelamiento del flujo de aire forzado en un invernadero. *Facultad de Ingeniería en Ciencias Aplicadas*, (Trabajos Titulación Pregrado), Ibarra, Ecuador, 2019. (In Spanish) http://repositorio.utn.edu.ec/handle/123456789/9366

[13] J.G. Paredes Salinas, C.F. Pérez Salinas, C.B. Castro Miniguano, Análisis de las propiedades mecánicas del compuesto de matriz poliéster reforzado con fibra de vidrio 375 y cabuya aplicado a la industria automotriz. *Enfoque UTE*, 8(3), 2017: 1-15. (In Spanish)

[14] J. Xamán, M. Gijón-Rivera, Dinámica de fluidos computacional para ingenieros. *Palibrio*, Indiana, United States, 2016.

[15] J. Jiménez, Turbulence and vortex dynamics, Madrid and Stanford, 2004. (Accessed: 26 February 2024) https://torroja.dmt.upm.es/area_alumnos/Introduccion_a_la_turbulencia/apuntes.pdf

[16] L. Davidson, Fluid mechanics, turbulent flow and turbulence modeling. *CFD Course*, 2012: 1-270. (Accessed: 18 December 2023 ) https://www.tfd.chalmers.se/~lada/comp_turb_model/postscript_files/solids-and-fluids_turbulent-flow_turbulence-modelling_12.pdf

[17] J. Franke, A. Hellsten, H. Schlünzen, B. Carissimo, Best practice guideline for the CFD simulation of flows in the urban environment. *COST European Cooperation in Science and Technology*, 2007: hal-041813902007. https://sciencespo.hal.science/ENPC-CEREA/hal-04181390v1

[18] F.S. Chiwo, A.d.C. Susunaga-Notario, J.A. Betancourt-Cantera, R. Pérez-Bustamante, V.H. Mercado-Lemus, J. Méndez-Lozoya, G. Barrera-Cardiel, J.E. García-Herrera, H. Arcos-Gutiérrez, I.E. Garduño, Design and Optimization of the Internal Geometry of a Nozzle for a Thin-Slab Continuous Casting Mold. *Designs*, 8(2), 2024: 2. https://doi.org/10.3390/designs8010002

[19] H. Salehi, H. Basir, H.M. Bidhend, F. Farhani, M.A. Rosen, Experimental and simulation study of an automobile cooling system: Performance improvement using passive flow control. *International Communications in Heat and Mass Transfer*, 149, 2023: 107168. https://doi.org/10.1016/j.icheatmasstransfer.2023.107168

[20] J.D. Viana-Fons, J. Payá, Dynamic cabin model of an urban bus in real driving conditions. *Energy*, 288, 2024: 129769. https://doi.org/10.1016/j.energy.2023.129769

[21] T. Kobayashi, M. Tsubokura, CFD application in automotive industry. 100 Volumes of 'Notes on Numerical Fluid Mechanics'. *Notes on Numerical Fluid Mechanics and Multidisciplinary Design*, 100, 2009: 285-295. https://doi.org/10.1007/978-3-540-70805-6_22

[22] C. Zhang, M. Uddin, A.C. Robinson, L. Foster, Full vehicle CFD investigations on the influence of front-end configuration on radiator performance and cooling drag. *Applied Thermal Engineering*, 130, 2018: 1328-1340. https://doi.org/10.1016/j.applthermaleng.2017.11.086

[23] F. Wang, A New System Restriction Simulation Method for Underhood Airflow CFD Analysis. SAE Technical Paper. 2007-01-0768. *SAE Internationa*l, 2007.

[24] E. Rusly, L. Aye, W.W.S Charters, A. Ooi, CFD analysis of ejector in a combined ejector cooling system. *International Journal of Refrigeration*, 28(7), 2005: 1092-1101. https://doi.org/10.1016/j.ijrefrig.2005.02.005

[25] H.A. Hasan, H. Togun, A.M. Abed, H.I. Mohammed, N. Biswas, A novel air-cooled Li-ion battery (LIB) array thermal management system–a numerical analysis. *International Journal of Thermal Sciences*, 190, 2023: 108327. https://doi.org/10.1016/j.ijthermalsci.2023.108327

[26] T. Gammaidoni, J. Zembi, M. Battistoni, G. Biscontini, A. Mariani, CFD Analysis of an Electric Motor's Cooling System: Model Validation and Solutions for Optimization. *Case Studies in Thermal Engineering*, 49, 2023: 103349. https://doi.org/10.1016/j.csite.2023.103349

[27] D.Y. Kim, H.C. No, A CFD-based design optimization of air-cooled passive decay heat removal system. *Nuclear Engineering and Design*, 337, 2018: 351-363. https://doi.org/10.1016/j.nucengdes.2018.07.008

[28] L. Tan, Y. Yuan, L. Tang, C. Huang, Numerical simulation on fluid flow and temperature prediction of motorcycles based on CFD. *Alexandria Engineering Journal*, 61(12), 2022: 12943-12963. https://doi.org/10.1016/j.aej.2022.07.001

[29] A. Ašonja, E. Desnica, I. Palinkaš, Analysis of the static behavior of the shaft based on finite element method under effect of different variants of load. *Applied Engineering Letters*, 1(1), 2016, 8-15.